Abeer Mohammed *et al.*
Environmental Sciences Europe 2022, **34**(1):109
https://doi.org/10.1186/s12302-022-00684-2

Environmental Sciences Europe

RESEARCH

Open Access

The potential activity of biosynthesized silver nanoparticles of *Pseudomonas aeruginosa* as an antibacterial agent against multidrug-resistant isolates from intensive care unit and anticancer agent

A. B. Abeer Mohammed[1], Mona Mohamed Abd Elhamid[2], Magdy Kamal Mohammed Khalil[3], Abdallah Soubhy Ali[4*] and Rateb Nabil Abbas[1]

Abstract

Background: Antibiotic resistance is a global problem; especially the multidrug-resistant bacteria are a serious and fatal problem in the intensive care unit. Interestingly, biosynthesized silver nanoparticles are the promising key to eliminate these microbes. Using *Pseudomonas aeruginosa* supernatant is an easy and cheap method in silver nanoparticle biosynthesis. The biosynthesis conditions were adjusted, and the profiling of the biosynthesized silver nanoparticles was confirmed.

Results: The UV spectroscopy at a wavelength at 400 nm was 0.539 A.U., transmission electron microscope showed nanoparticles were homogeneous with a square and spherical shape, its average size 20 nm, The capping material and the existence of silver nanoparticles were confirmed using Fourier transform infrared spectroscopy, and energy dispersive *X*-ray spectroscopy. The minimum inhibitory concentration was 1 mg/ml against multidrug-resistant bacteria, and LC50 was 62.307 µg/ml on the hepatocellular carcinoma cell line.

Conclusions: Microbial-synthesized silver nanoparticles have a potential application to combat multidrug-resistant bacteria, especially in the intensive care unit.

Keywords: Silver nanoparticles, Multidrug-resistant bacteria, *Pseudomonas aeruginosa*, Cytotoxicity, Hepatocellular carcinoma

Background

Antibiotic resistance is a global problem, due to increasing the types of microorganisms that resist all types of antibiotics. However, there is a limited production of new antibiotic lines, so using new materials like nanoparticles (NPs) which have high antibacterial activity, is a promising solution to this problem. Multidrug-resistant (MDR) bacteria are a serious and fatal problem in the intensive care unit (ICU). During ICU admission, these bacteria infect more than 50% of the patients, and up to 64% of the patients were infected via inhalation and aspiration. The main infectious pathogens in the ICU classified as 62.2% were Gram-negative bacteria (GNB) and 37.8% were Gram-positive bacteria (GPB). The common infectious species are *Enterococcus faecium, Enterobacter* spp., *Acinetobacter baumannii, Klebsiella pneumoniae, P. aeruginosa,* and *Staphylococcus aureus* [1, 2].

*Correspondence: abdallah.ali@agr.cu.edu.eg

[4] Department of Microbiology, Faculty of Agriculture, Cairo University, Giza 12613, Egypt
Full list of author information is available at the end of the article

© The Author(s) 2022, corrected publication 2023. **Open Access** This article is licensed under a Creative Commons Attribution 4.0 International License, which permits use, sharing, adaptation, distribution and reproduction in any medium or format, as long as you give appropriate credit to the original author(s) and the source, provide a link to the Creative Commons licence, and indicate if changes were made. The images or other third party material in this article are included in the article's Creative Commons licence, unless indicated otherwise in a credit line to the material. If material is not included in the article's Creative Commons licence and your intended use is not permitted by statutory regulation or exceeds the permitted use, you will need to obtain permission directly from the copyright holder. To view a copy of this licence, visit http://creativecommons.org/licenses/by/4.0/.

Biosynthesis methods are the most promising and efficient among numerous synthetic ways for silver nanoparticles (AgNPs). The main advantages of the biosynthesis methods are rapid, easy, and non-toxic, which can form the AgNPs with well-defined size, high stability and solubility, and high yield by optimizing the biosynthesis conditions [3]. The biosynthesis of AgNPs has extensively studied the mode of action as antimicrobial and cytotoxic activity against pathogenic bacteria. Microbial biosynthesis of the AgNPs using the supernatant is an easy and cheap method to synthesize NPs with specific size and morphology shapes. Microbial products such as enzymes, proteins, and bio-surfactants are the key to capping and/or stabilizing of the NPs in the biosynthesis process [4]. In addition, biosynthesized AgNPs are more acceptable for biomedical applications than chemical synthesized AgNPs [5].

Pseudomonas is an opportunistic pathogen commonly found in soil and aquatic environment. Many *Pseudomonas* species can grow under different environmental conditions, facultatively anaerobic, and oxidize glucose and xylose. However, it cannot ferment lactose and other carbohydrates, and it can use nitrate as an inorganic electron acceptor [6]. The most common species of human infection is *P. aeruginosa*, which can cause infections in the blood, lungs (pneumonia), and skin, particularly in the immunocompromised patients post-surgery.

Several reports showed that AgNPs are effective against pathogenic organisms. The antibacterial activity of the biosynthesized AgNPs against several pathogenic bacteria, such as, *P. aeruginosa*, *Salmonella paratyphi*, *B. subtilis*, *K. pneumoniae*, *E. coli* and *Staph. aureus*, was reported by Mohammed et al. [7], Bindhu et al. [8] and Prasad and Elumalai [9]. The antimicrobial activity of AgNPs is directly proportional to the surface area of the particles exposed to the interaction, which facilitates the mechanical penetration of the cell membrane and increases the adhesion to the surface of microbial cells better. An additional mechanism of antimicrobial AgNPs-based via forming of diverse reactive oxygen species (ROS) can destroy cell envelope, enzymes, intracellular substances, and DNA [10–12]. Meanwhile, ROS increases the cytotoxicity of AgNPs by reducing the metabolic activity, ATP content, and oxidative stress, damaging the mitochondria and decreasing cell viability. The cytotoxicity of AgNPs was confirmed inside the mitochondria and nucleus using the transmission electron microscopic (TEM), as reported by AshaRani et al. and Xue et al. [13, 14].

This study investigates the antibacterial efficacy of *P. aeruginosa* EGY1 biosynthesized AgNPs on MDR bacteria from ICU and cytotoxicity using hepatocellular carcinoma cell line. The production and physicochemical characterization of AgNPs have been studied for *P. aeruginosa*.

Materials and methods

Ethical statement

This protocol was approved by the Ethics Committee of the First Affiliated Hospital of National liver institute Menoufia University (eNLI IRB Protocol number: 00180/2019).

Specimen collection, bacterial identification, and antibiotic susceptibility

The bacterial isolates were collected from ICU patients in the National Liver Institute at the main Hospital of Menoufia University, Menoufia, Egypt. The specimen was collected according to the guidelines of the European Committee on Antimicrobial Susceptibility Testing (EUCAST) from January 2019 to June 2020, for a period of 1.5 years. The samples were collected from blood, urine, sputum, ascetic fluid, and wounds, the bacterial isolation and identification according to the guidelines of the European Committee on Antimicrobial Susceptibility Testing (EUCAST) [15]. All isolates were cultured onto MacConkey and blood agar, then incubated at 37 °C for 24 h to make sure of purity and viability. Bacterial isolates were identified using Gram stain and VITEK-2 system version 08.01 bioMerieux to profiling the characterizations of bacterial isolates and antibiotic susceptibility, and cards were used according to the manufacturer's instructions. Suspensions of microbial culture were prepared in 0.9% of NaCl solution, and the optical density was adjusted to 0.63 McFarland units using a Densichek system (bioMérieux) [16]. The extended-spectrum β-lactamase (ESBL) were identified based on the results of VITEK-2 and according to the classification scheme for ß-lactamases reported by BUSH et al. [17], Bradford [18] and Lee et al. [19]. The bacterial strain was stored in 20% glycerol, nutrient broth agar at −20 °C for further experiments [20].

Molecular identification of the bacterial isolate

The partial sequencing-based 16S rRNA gene method was used to identify the selected isolate [21]. The DNA of the selected isolate was extracted using the extraction kit of genomic DNA (Intron, Biotechnology, Korea). The PCR amplification of 16S rDNA was done using universal primers (***5′AGA GTT TGA TCC TGG CTC AG 3′*** (20 mer) for **27F**-forward primer and ***5′CTA CGG CTA CCT TGT TAC GA 3′*** (20 mer) for the **1492R**-reverse primer) using the thermal cycler (Thermo Fisher Scientific, USA) for 35 cycles as follows; at 95 °C for 5 min for the initial denaturation, at 94 °C for 35 s. For denaturation, at 57 °C for 30 s. for annealing, at 72°C for 1 min for extension,

and finally, the extension was at 72 °C for 10 min. The quality of the selected isolate's amplicons (PCR product) was verified by electrophoresis on a 1% agarose gel and compared with 1 kb DNA ladder (Intron Biotechnology, Korea). The electrophoresis run was performed in 1x Tris–borate–EDTA (TBE) buffer at 80 V for 40 min in a Bio-Rad submarine (8 × 12 cm), stained with ethidium bromide. Then, visualizing the 16S gene amplicons' DNA banding patterns was tested under UV light by UV-transilluminator (Thermo Fisher Scientific, USA). The purification of PCR products was applied according to the manufacturer's instructions of the genomic DNA purification kit (gene JET™, Intron Biotechnology, Korea). The sequencing of the PCR products was performed using forward and reverse primers with ABI 3730xl DNA sequences. The sequences of PCR product were identified with accession number MT071505 and compared with similar sequences from the GenBank database using NCBI and BLAST (https://www.ncbi.nlm.nih.gov/nuccore/MZ936999.1). Also, the phylogenetic analysis was formed by using BLAST tools.

Preparation of bacterial supernatant

Fresh culture of *P. aeruginosa* isolate was inoculated in nutrient broth (NB) in sterilized test tubes (10 ml) in parallel with a control (NB media without inoculation) and incubated for 24 h at 37 °C in a rotary shaker incubator at 150 rpm. After the incubation, the culture was centrifuged for 10 min at 6000 rpm to obtain cell-free filtrate (CFF). The supernatant was collected for further experiments, but the pellet was discarded.

Extracellular synthesis of silver nanoparticles

Silver nitrate (from sigma Aldrich company) 1 mM concentration was added to the *P. aeruginosa* supernatant (CFF) under sterilized conditions, and the tubes were monitored at a regular interval for a color change for 48 h. The formed AgNPs were dried and obtained as a powder for further characterization and antimicrobial studies [22, 23].

Optimization of silver nanoparticles synthesis

Microbial synthesis of AgNPs by the supernatants (CFF) of *P. aeruginosa* was investigated under different conditions to identify the optimum conditions for bio-reduction of silver ions. The supernatant was added at different concentrations (10, 25, 50% of total mixture volume), different concentrations of $AgNO_3$ (1, 2 and 4 mM), at different pH range (4, 7, 8) and incubation temperature (28–37 and 50 °C) using 1 mM of silver nitrate, 25% of bacterial supernatant at different pH and temperature, 0.2 M NaOH and 0.1 M HCl for 48 h incubation time [24].

Characterization of AgNPs

UV–Vis spectrophotometer analysis

The biological reduction of the Ag+ ions was measured using the UV–Vis spectroscopy (T80 + UV–Vis Spectrometer) and scanning between 200 and 800 nm at 25 °C and aliquots (2 mL of the reaction mixture).

Field emission transmission electron microscopy (FE-TEM)

The size, shape, assembly, elemental compositions, and purity of the synthesized AgNPs were identified using transmission electron microscopic (TEM) analysis (JEOL JEM-2100) at Science Faculty Menoufia University, Egypt. The samples were prepared for TEM studies by placing two drops of sterilized dispersed AgNPs mixture onto carbon-coated TEM grids. The TEM grid containing the samples were dried and transferred to the microscope at room temperature. Using FE-TEM, energy dispersive aTEM-2100 F(JEOL) and operated at 200 kV.

X-ray diffraction (XRD)

The XRD investigations were carried out using a D8-Advance *X*-ray diffractometer (Bruker, Germany), which was operated at 40 kv, m A, with Cu Kα radiation, at 6°/min a scanning rate, with a step size of 0.02, across a 2θ range of 20–80°. The samples were centrifuged and stored at 80 °C for 2 h, then lyophilized and pulverized the AgNPs samples before being used in XRD. X-ray crystallography was used to estimate the crystalline phase of the nanoparticles. The size of nanoparticles was obtained by Debye–Scherrer's formula:

$$D = K\lambda/(\beta \mathrm{COS}\,\theta), \tag{1}$$

where D is the crystal size, λ is the X-ray radiation wavelength of CuKα (= 0.15406 nm), $K = 0.89$, and β is the line width at half-maximum height [25].

Fourier transform-infrared (FT-IR) spectroscopy

IR spectral analyses identify the biomolecules responsible for the bio-reduction, the stabilization and capping of Ag NPs. The samples were pulverized for FTIR analysis using the freeze-dried. The spectra were measured from 400 to 4000 cm^{-1} at a resolution of 4 cm^{-1} using a Perkin Elmer FTIR-spectrometer.

Antimicrobial activity of Ag NPs

Well diffusion assay (WD assay)

The antibacterial activity of AgNPs was assessed using the WD assay method. The tested microorganisms *K. pneumonia, P. aeruginosa,* and *A. baumannii* were grown overnight in Luria broth (LB), 100 µL culture of each strain was conveyed on the surface of the LB agar plate. The wells were created on the surface of the LB agar plate using a sterile cork borer [26], each well (8 mm) contains

100 µL of Ag NPs (0.5 mg/ml dissolved in water). AgNPs formed with silver nitrate concentration 1 mM and pH 7 at well A, 2 mM and pH 7 at well B, 4 Mm and pH 7 at Well C, 1 Mm and pH 8 at Well D, Well E for silver nitrate solution as a control. All plates were incubated at 37 °C for 24 h. The antibacterial activity of AgNPs were compared to some commercial antibiotics alone (ciprofloxacin, cefotaxime, and cefazolin). In combination with formed AgNPs by disc diffusion method, paper discs (6 mm) containing 50 µL of the Ag NPs (0.5 mg/ml in water) and incubation at the same conditions then measured the inhibition zones. The experiments were carried out in triplets to calculate the standard deviation.

Minimum inhibitory concentration (MIC)

The antibacterial effectiveness of the AgNPs was assessed using the standard tube dilution method on LB medium. The pathogenic bacteria (*A. baumannii, P. aeruginosa, and K. pneumoniae*) were inoculated and cultured overnight at 37 °C under shaking at 150 rpm. The cultured bacteria were diluted to $5^{*}10^{6}$ CFU/ml and incubated at 37 °C for 10 min. The concentrations of AgNPs were prepared using 1 mM of silver nitrate, 25% of bacterial supernatant, pH 7 and applied to bacterial suspensions were 50, 100,150, and 200 ppm, respectively. Following EUCAST's instructions (2003), bacterial growth was observed after 24 h of incubation. The minimal inhibitory concentration (MIC) of Ag-NPs that reduced bacterial growth to 99.9% was determined after culturing the tested bacteria on LB agar for 24 h at 37 °C. The optical density of the incubated tubes with AgNPs was measured at 600 nm [27].

Cytotoxicity assay

The bioactivity of AgNPs on the viability of the cell was measured using Sulforhodamine B die (SRB assay). In 96-well plates, aliquots of 100 L Hep G2 Hepatocellular carcinoma cell line suspension (5×10^3 cells) were cultured in a complete medium overnight. An additional aliquot of 100 µL media with AgNPs was given to the cells at various doses (10 and 100 µg/ml). After 72 h of AgNPs treatment, the media were replaced with 150 µL of 10% trichloroacetic acid (TCA) to fix the cells after incubating for 1 h at 4 °C. The cells were washed five times with di.H_2O to remove the TCA solution from the cells. SRB solution (0.4% w/v) was added as aliquots (70 µL) and incubated for 10 min at 25 °C. The plates were washed 3-times with 1% CH_3COOH and saved overnight for air-dried. Finally, the protein-bound SRB stain was dissolved into 150 µL of TRIS solution (10 mM) and measured the absorbance at 540 nm using an Omega microplate reader (BMGLABTECH®- FLUO star, Ortenberg, Germany) [28].

Statistical analyses

Statistical analysis of all experiments was computed using Microsoft Excel from the mean of three trials and the differences were considered significant when $p < 0.01$.

Results

Bacterial identification and antibiotic susceptibility

A total of 273 isolates were screened from the ICU patients. The types of isolated pathogens are mentioned in Table 1, of which 227 isolates (83.15%) were GNB. Among these GNB there are 64.46% identified as *K. pneumonia*, these isolates contained 21.97% as extended-spectrum β-lactamase (ESBL) resistance strains, and 15.38% were classified as carbapenemase-producing Enterobacteriaceae (CRE) strains. The *Escherichia coli represent* (8.42%) of this specie; about 2.19% are classified as (ESBL) and 2.19% as (CRE). Also, *P. aeruginosa* was (3.66%), *Proteus mirabilis* (3.30%), *Acinetobacter* species (2.56%), and *Salmonella* species (0.73%). Likewise, up to 46 isolates (16.85%) identified as GPB, 5.49% were *Staph. aureus*, 8.79% were *Streptococcus* species, and 2.56% were *Enterococcus* species, as mentioned in Table 1.

The identification and antibiotic susceptibility tests were confirmed using the VITEC-2 system. All selected strains were classified as MDR bacteria with high resistance to all tested antibiotics ß-lactam, cephalosporins,

Table 1 Bacterial isolates percent from infected patients in the critical care unit

Organisms	ESBL	CRE	Non-ESBL&-CRE	Number	Percent*(%)
Facultative and aerobic GNB					
Klebsiella species	*60*	*42*	*74*	176[a]	64.4
E. coli	*6*	*6*	*11*	23[ab]	8.42
P. aeruginosa				10[b]	3.66
Proteus mirabilis				9[b]	3.30
Acinetobacter species				7[b]	2.56
Salmonella species				2[ab]	0.73
Total				227	83.15
Facultative aerobe GPB					
Staph. aureus				15[c]	5.49
Streptococcus species				24[c]	8.79
Enterococcus species				7[c]	2.56
Total				46	16.85

GNB, Gram-negative bacteria; GPB, Gram-positive bacteria; ESBL extended-spectrum β lactamase resistance strains; CRE carbapenemase-producing Enterobacteriaceae strains

* Percent of strains divided into the total number of strains

[a, b, c] Different letters indicate significant differences among strains according to the Tukey-Kramer test at $p < 0.01$

Table 2 Minimum inhibitory concentration (mic) and antibiotic susceptibility of *P. aeruginosa*

Antibiotics tested	Isolates MIC (mg/L)	MIC breakpoint (mg/L)	
		≤	R >
β-lactams			
AMP	≥ 32	8	8
CFZ	≥ 64	16	16
CTR	≥ 64	1	1
CAZ	≥ 64	1	4
CFX	≥ 64	1	2
CPM	≥ 64	1	4
β-lactam/			
AMS	≥ 32	8	8
β-lactamase inhibitor			
TZP	≥ 128	8	16
Carbapenems			
MEM	≥ 16	2	8
Aminoglycosides			
AMK	≥ 64	8	16
GEN	≥ 16	2	4
TOB	≥ 16	2	4
Quinolones			
CIP	≥ 4	0.06	0.06
LEV	≥ 8	1	2
Others			
NIT	≥ 512	4	64
SXT	≥ 320	2	4

AMP, ampicillin; CFZ, cefazolin; CTR, ceftriaxone; CAZ, ceftazidime; CFX, cefoxitin; CPM, cefepime; AMS, ampicillin/sulbactam; TZP, 182 piperacillin/tazobactam; MEM, meropenem; AMK, amikacin; GEN, gentamicin; TOB, tobramycin; CIP, ciprofloxacin; LEV, levofloxacin; NIT, nitrofurantoin; SXT, Trimethoprim / Sulfamethoxazole

quinolone, aminoglycosides, macrolides, and carbapenems. The antibiotic susceptibility of MDR *P. aeruginosa* isolates and MIC are listed in Table 2. Phenotypic identification of *P. aeruginosa* was done by the VITEC-2 automated system, and the results are present in Table 3.

Molecular identification and phylogenetic analysis

Molecular identification using the 16S rRNA gene is the easiest, and fastest technique used widely for the microbial identification and evaluation of the phylogenetic relationships between microorganisms. Sequencing of the 16S rRNA gene has been employed to aid the differential identification among the species of *Pseudomonas*.

The size of the amplified PCR product extracted from the selected isolates was (1391 bp). The sequences of the selected isolate "EGY1" was compared with the identified sequences in the NCBI GenBank database and showed the highest percentage of similarity (97.05%) with *P. aeruginosa* strain NBRC 1268 under accession no. MZ936999 and the significant matches with hi max score were 1982, zero e-value, and 97.05% nucleotide identity for isolate EGY1. The phylogenetic tree presented in Fig. 1 reveals a strong genetic relationship between the Egyptian isolate of *P. aeruginosa* EGY1 and *P. aeruginosa* strain NBRC 1268, which strongly confirms its identity as *P. aeruginosa*.

Biosynthesis of AgNPs using cell-free filtrate supernatant

The biosynthesis of AgNPs can be identified using a visual indicator that can be seen by changing the color of the reaction. Bio-formation of AgNPs from the mixture of $AgNO_3$ using microbial supernatants was monitored visually as the primary indicator of the biosynthesis

Table 3 VITEK-2 identification result of *P. aeruginosa*

Well	Test	Result	Well	Test	Result	Well	Test	Result	Well	Test	Result	Well	Test	Result
2	APPA	−	3	ADO	−	4	PyrA	−	5	IARL	−	7	dCEL	−
9	BGAL	−	10	H2S	−	11	BNAG	−	12	AGLTp	−	13	dGLU	+
14	GGT	+	15	OFF	−	17	BGLU	−	18	dMAL	−	19	dMAN	+
20	dMNE	+	21	BXYL	−	22	BAlap	+	23	ProA	+	26	LIP	+
27	PLE	−	29	TyrA	+	31	URE	−	32	dSOR	−	33	SAC	−
34	dTAG	−	35	dTRE	−	36	CIT	+	37	MNT	+	39	5 KG	−
40	ILATk	+	41	AGLU	−	42	SUCT	+	43	NAGA	−	44	AGAL	−
45	PHOS	−	46	GlyA	−	47	ODC	−	48	LDC	−	53	IHISa	−
56	CMT	+	57	BGUR	−	58	O129R	+	59	GGAA	−	61	IMLTa	+
62	ELLM	−	64	ILATa	+									

APPA, Ala-Phe-Pro-arylamidase; ADO, adonitol; PyrA, L-pyrrolydonyl-arylamidase; IARL, L-arabitol; dCEL, D-cellobiose; BGAL, beta-galactosidase; H2S, H2S production; BNAG, beta-N-acetyl-glucosaminidase; AGLTp, glutamyl arylamidase pNA; dGLU, D-glucose; GGT, gamma-glutamyl-transferase; OFF, fermentation/ glucose; BGLU, beta-glucosidase; dMAL, D-maltose; dMAN, D-mannitol; dMNE, D-mannose; BXYL, Beta-xylosidase; BAlap, beta-alanine arylamidase pNA; ProA, L-proline arylamidase; LIP, lipase; PLE, palatinose; TyrA, tyrosine arylamidase; URE, urease; dSOR, D-sorbitol; SAC, saccharose/sucrose; dTAG, D-tagatose; dTRE, D-trehalose; CIT, CITRATE (Sodium); MNT, malonate; 5 KG, 5-keto-D-gluconate; ILATk, L-lactate alkalinization; AGLU, alpha-glucosidase; SUCT, succinate alkalinization; NAGA, Beta-N-acetyl-galactosaminidase; AGAL, alpha-galactosidase; PHOS, phosphatase; GlyA, glycine arylamidase; ODC, ornithine decarboxylase; LDC, lysine decarboxylase; IHISa, L-histidine assimilation; CMT, coumarate; BGUR, beta-glucuronidase; O129R, O/129 resistance (comp.vibrio.); GGAA, Glu-Gly-Arg-arylamidase; IMLTa, L-malate assimilation; ELLM, Ellman; ILATa, L-lactate assimilation

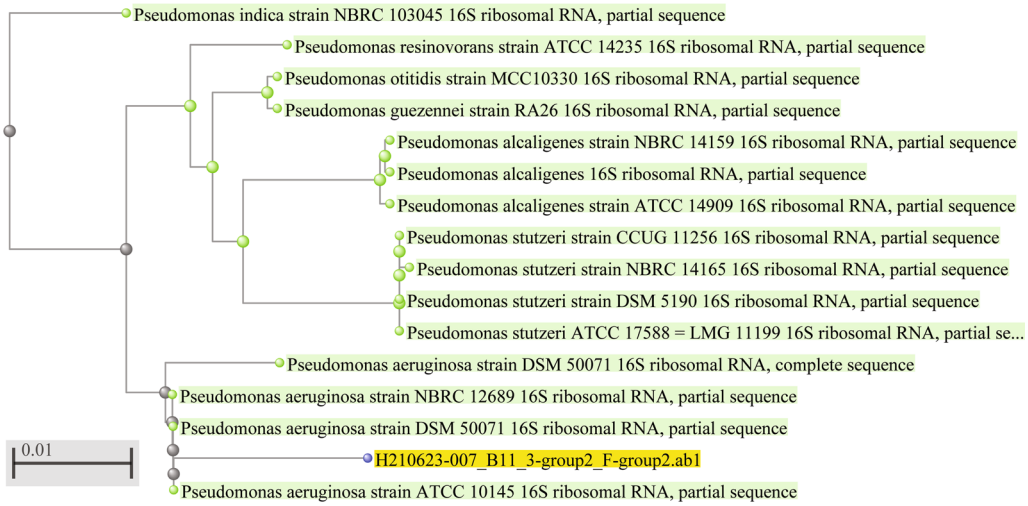

Fig. 1 Phylogenetic tree of Egyptian bacterial isolate of *P. aeruginosa* EGY1 and selected strains of identified *P. aeruginosa*

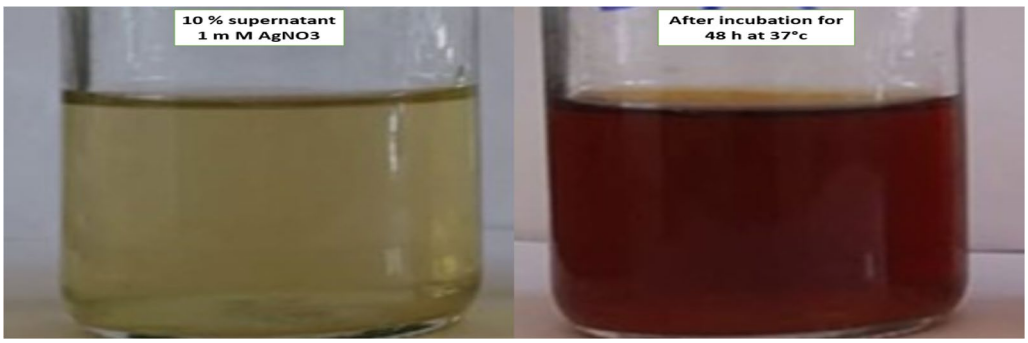

Fig. 2 The bacterial supernatant with 10% of supernatant and 1 mM of $AgNO_3$ before and after incubation for 48 h. The biosynthesis confirmed by changing the color of the reaction as a visual indicator

process (Fig. 2). The transition of the color from yellow to brown in the presence of bacterial supernatants, is a primary indicator of the biotransformation of Ag^+ ion to Ag^0. In contrast, there is no change of color in the control media, which indicates that compounds in the media did not affect the reduction of Ag^+ ion. The reduction mechanism and biosynthesis process of AgNPs using the supernatant of *P. aeruginosa* was confirmed by the appearance of the surface plasmon peak at 300 to 400 nm using the UV–vis measurement (Fig. 3). These results showed only in bacterial supernatant and $AgNO_3$. In contrast with neither bacterial extract nor $AgNO_3$ solution, no absorption band was seen.

Optimization of AgNPs biosynthesis

The conditions of biosynthesis have a significant effect on final synthesized nanoparticles. The effect of the biosynthesis of AgNPs at the different volumes of bacterial supernatant (Fig. 4A), $AgNO_3$ concentration (Fig. 4B), and pH (Fig. 4C).

The volume of supernatant is one of the significant parameters that control the size and shape of NPs and thus influences their properties. It has effects on reaction time and the color of the reaction mixture. The volume of bacterial supernatant was added at 10, 25, and 50% of the total volume as 1:9, 2.5:7.5 and 5:5 ratios, respectively. Figure 4 A, B shows the visual color of the final mixture after incubation at different volumes of bacterial supernatant. The reaction mixture contained 25% supernatant, had the darkest color intensity than 50% and 10% of supernatant volume. The absorbance

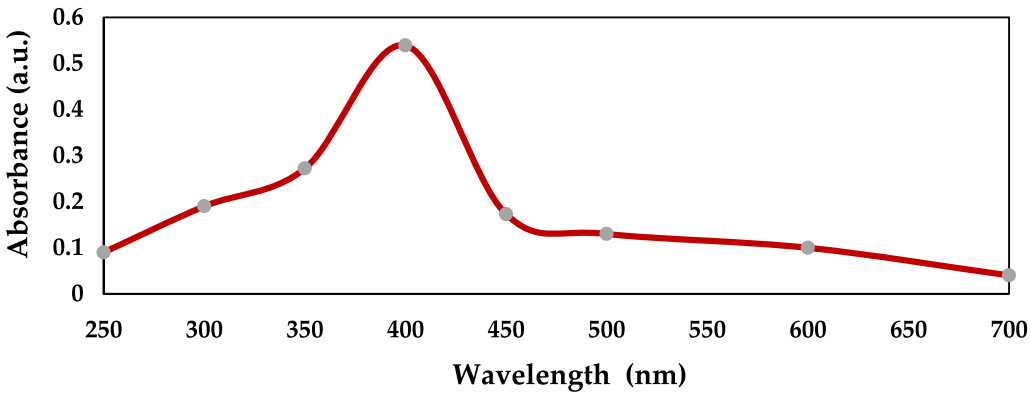

Fig. 3 UV–vis absorbance (arbitrary units, a.u.) curve of the reaction mixture after incubation. The maximum absorbance peak of surface plasmon of AgNPs present at 400 nm

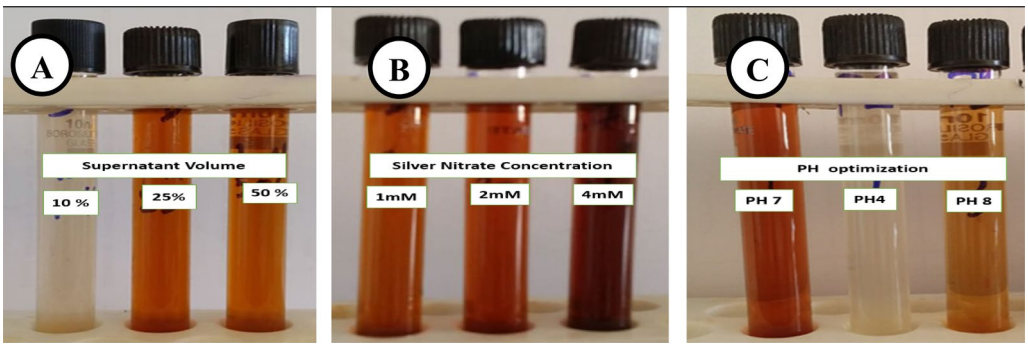

Fig. 4 Optimization of nanoparticles synthesis at **A** different volumes of bacterial supernatant, **B** $AgNO_3$ concentration, and **C** mixture pH. The biosynthesis confirmed by changing the color of the reaction as a visual indicator

peaks of *P. aeruginosa* at supernatant volume 10%, 25% and 50% were 0.193 A.U., 0.29 A.U., 0.539 A.U., respectively. Interestingly to mention that the UV–vis absorption intensity was higher for the AgNPs synthesized using 50% supernatant volume than 10% volume with absorbance beak 0.193 nm and 25% supernatant volume with absorbance beak 0.29 nm, as in Fig. 5A.

Silver nitrate concentration was added in three different concentrations 1 mM, 2 mM, and 4 mM. There are no significant visual changes in the color of the final prepared mixture, as shown in Fig. 4. However, UV–vis absorbance intensity was 0.2 A.U. 0.621 A.U., and 0.956 A.U. for *P. aeruginosa* for the three concentrations, respectively. The maximum absorbance was at 4 mM silver nitrate concentration, as in Fig. 5B.

The optimization of biosynthesis conditions by changing the pH of the final mixture to pH 4, 7, and 8, which directly affect the biosynthesis of AgNPs. The changes in pH significantly affecting the color of the final mixture of *P. aeruginosa*, which gave absorbance after the incubation for 48 h were 0.178, 0.392, and 0.368 A.U., respectively in Fig. 5C. These results indicate that neutral pH is the most suitable pH for extracellular biosynthesis of AgNPs by bacterial filtrate. The highest intensity was recorded at wavelength 400–450 nm for pH 7 and 8. Contrariwise, there was almost no intensity at pH 4, indicating that this degree is not.

Characterization of AgNPs

Morphological and elemental profile of AgNPs using FE-TEM

The FE-TEM evaluated the morphological, essential profile and purity of the biosynthesized AgNPs. The morphological profile of biosynthesized AgNPs at 25% of *P. aeruginosa* supernatant and 1 mM of $AgNO_3$ formed homogenous particle size from 11 to 25 nm with an average size 18 nm, and well dispersed with different shape aspherical and square (Fig. 6A and B).

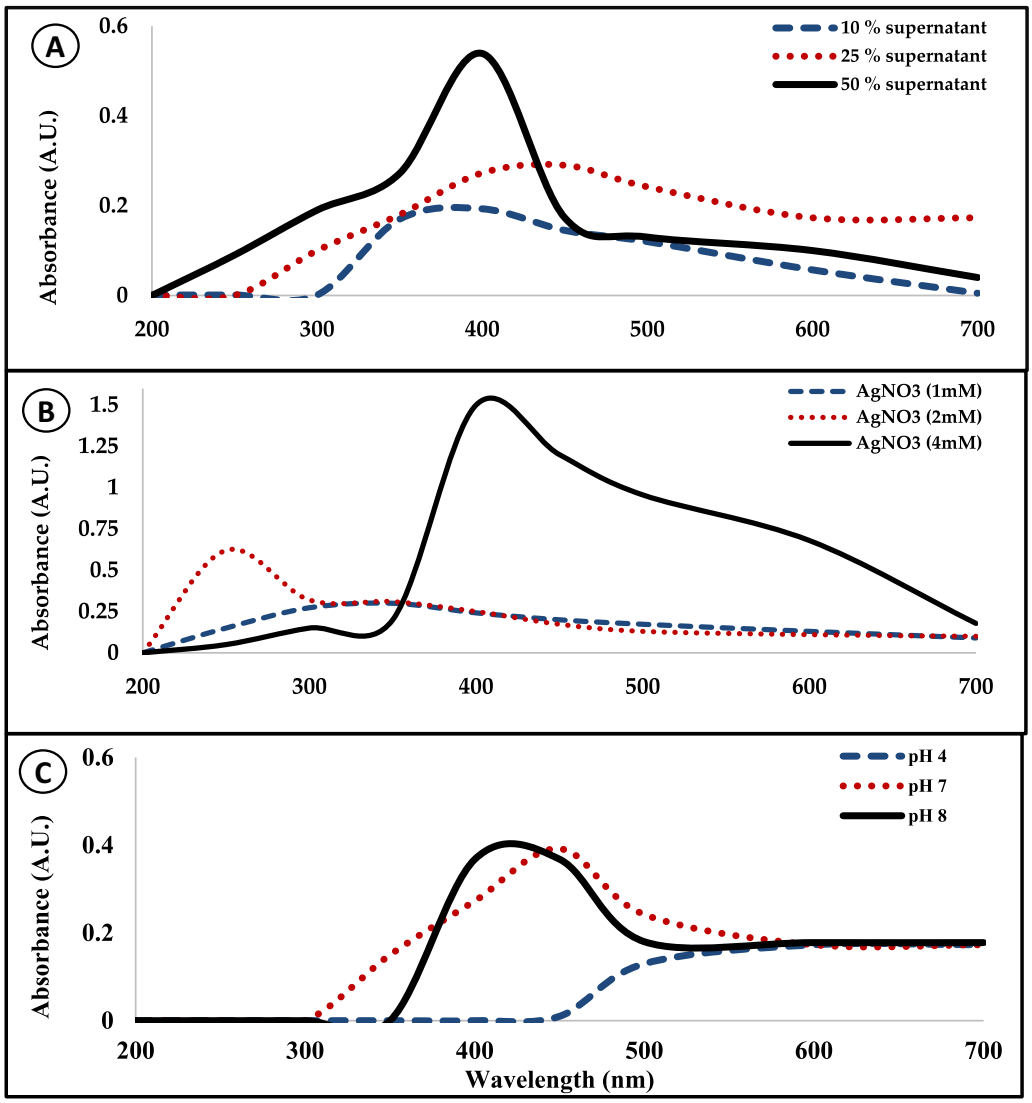

Fig. 5 Influence of the bacterial supernatant, $AgNO_3$ concentration and pH on the biosynthesis of AgNPs. A.U., arbitrary units. **A** Bacterial supernatant at different volumes 10, 25, and 50% (v/v), **B** $AgNO_3$ concentration (1, 2, and 4 mM), and **C** pH 4, 7 and 8. The maximum absorbance peak of surface plasmon of AgNPs was shifted based on the concentration and shape of AgNPs

X-ray diffraction (XRD)

The XRD identified the crystalline structure of biosynthesized AgNPs using the extracellular metabolites of *P. aeruginosa* and $AgNO_3$ solution (Fig. 7). The XRD patterns at 2 θ values 27.153°, 32.323°, 38.018°, 64.35°, and 43.934 indicated (110), (111), (210), (211), and (320), respectively, were the reflections of metallic silver. The diffraction patterns were analyzed and matched with the database of Joint Committee on Power Diffraction Standards (JCPDS) 03-0921, which confirmed these patterns of the metallic silver have the structure of face-centered-cubic (FCC). The crystallite size of AgNPs was determined according to the formula of *Debye–Scherrer*. The calculated particle size was 7.59519 nm and 11.63109 nm (Table 4). These results were matched with the FE-TEM results and confirmed with the database of JCPDS file no 03-092.

Fourier transform-infrared (FT-IR) spectroscopy

FTIR spectroscopy was used to identify the functional groups from the interaction between the metabolic components of *P. aeruginosa* and the metallic particles in Fig. 8. The spectrum of FTIR identified the unique peaks at 3431.48, 2926.11, 2862.46, 1648.23, 1397.47, 1110.07,

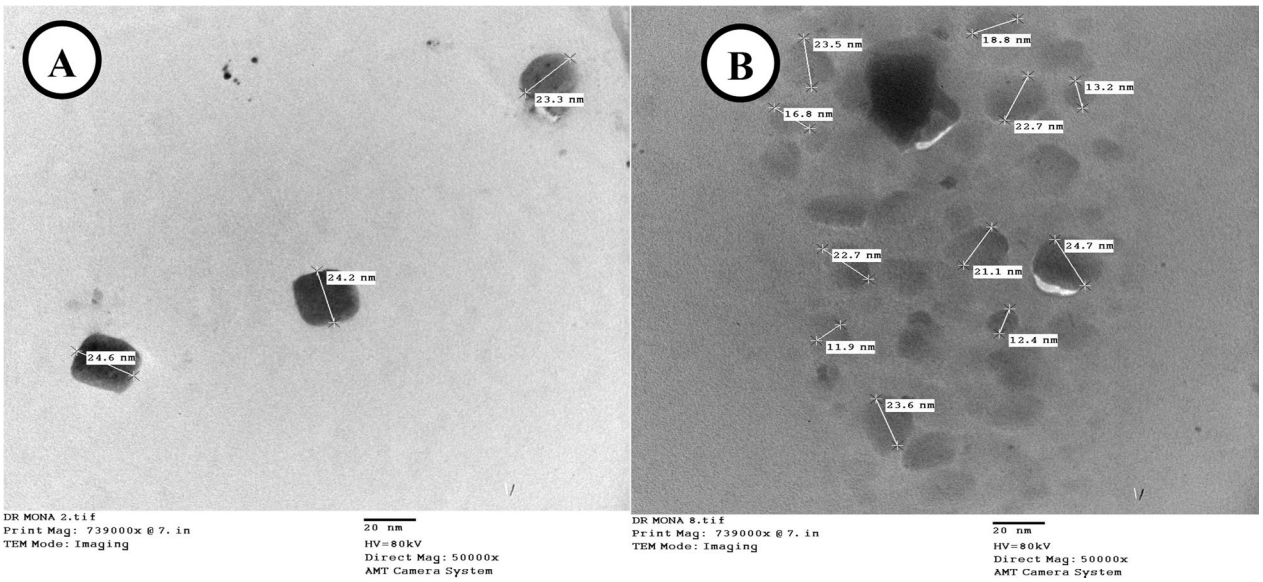

Fig. 6 TEM pictures of AgNPs synthesized by *P. aeruginosa* supernatant, **A** aspherical shape and **B** square shape. The average size was 18 nm

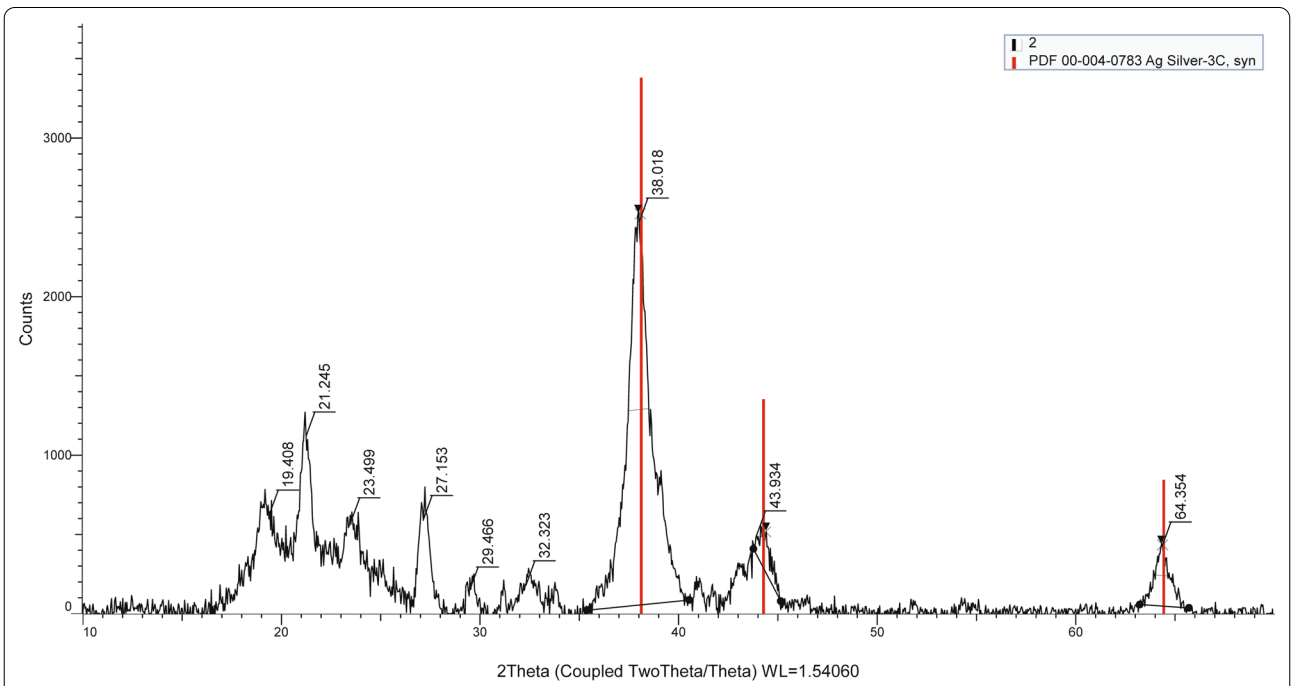

Fig. 7 XRD of silver nanoparticles formed by *P. aeruginosa* supernatant. The XRD patterns at 2 θ values 27.153º 32.323º, 38.018º, 43.934 and 64.35º, indicated to the reflections of metallic silver

Table 4 Calculation of nanoparticles particle size using Bragg's law

2 Theta	hkl	FWHM	D
38.018	210	1.094	7.59519
64.354	320	0.798	11.63109

1076.32 cm^{-1}. The peak at wave number 3431.48 cm^{-1} was attributed to the O–H stretching from the amide group, the peaks at 2926.11 cm^{-1} indicate to methylene group (CH_2), and the peak at 2289.58 cm^{-1} indicates CH_2 stretching. Also, the stretching of C=O from the amide I band of peptide linkage can be presented at 1648.23 cm^{-1}

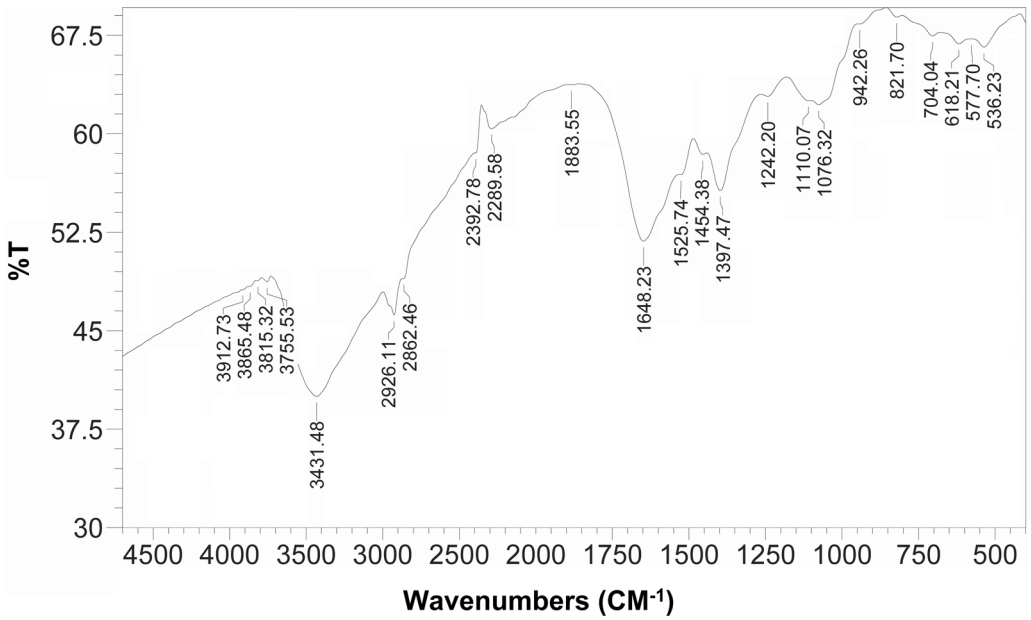

Fig. 8 FTIR of silver nanoparticles formed by *P. aeruginosa* supernatant. The spectrum of FTIR identified the unique peaks at 3431.48, 2926.11, 2862.46, 1648.23, 1397.47, 1110.07, 1076.32 cm^{-1}

Table 5 Well diffusion assay, antimicrobial activity of biosynthesized AgNPs at different concentrations of $AgNO_3$

Bacterial strain	Inhibition zone (mm)			
	$AgNO_3$ concentration			
	1 mM (A)	2 mM (B)	4 mM (C)	pH 8 (D)
A. baumannii	18 ± 0.18	16 ± 0.63	18 ± 0.85	14 ± 0.15
K. pneumonia	19 ± 0.14	17 ± 0.46	15 ± 0.23	14 ± 0.34
P. aeruginosa	19 ± 0.25	20 ± 0.92	22 ± 0.28	15 ± 0.09

[29]. The attributed peak at 1648.23 cm^{-1} represents symmetric stretching vibrations of carboxylate ion –COO– groups of the amino acid, and protein residues. The stretching vibrations of the carboxyl group C–O showed at peak 1397.47 cm^{-1}, as well as the stretching vibrations of C–O groups in the phenol, ether, or ester group attributed at peak 1110.07 cm^{-1}, likewise the stretching of the aromatic group presented at 1076.32 cm^{-1}. The peaks at 704.04 cm^{-1} and 618.21 cm^{-1} attributed to the OCN bending in the amide IV band arising, and the NH bending of peptide linkages in the amide V band arising identified at 821.70 cm^{-1} and the C=O of the amide VI bands arising presented at peak 536.23 cm^{-1}.

Antimicrobial activity of AgNPs

Well diffusion assay (WD assay)

The bioactivity of the biosynthesized AgNPs as the antibacterial agent was assessed using WDA, and the results were illustrated in Table 5. The maximum inhibition zones recorded with *A. baumannii* were 18 mm using AgNPs (1 and 4 mM). Furthermore, the maximum inhibition zone with *K. pneumoniae* was 19.17 mm at a concentration of 1 mM of AgNPs. Alongside *P. aeruginosa*, the maximum inhibition zone was 22 mm using 4 mM of AgNPs. The result approves the antibacterial activity of biosynthesized AgNPs formed from *P. aeruginosa* supernatant. There is no added benefit to increasing the concentration of $AgNO_3$ to form the nanoparticles as there is no significant difference between well A, B, and C. Changing of pH to 8 can decrease the antibacterial activity as shown by reducing the inhibition zone in well D, while there is no antibacterial activity for 1 Mm $AgNO_3$ solution alone. Interestingly, the combination of antibiotics and AgNPs recorded higher inhibition zone diameter for the combination disc than the antibiotic or nanoparticles alone, the antibiotics show no antibacterial activity against MDR bacteria in the current results in Table 6 and Fig. 9A–C.

Table 6 Inhibition zone of combination of nanoparticles and antibiotics ± SD

Bacterial strains	Inhibition zone (mm)					
	CIP	CIP + AgNPs	CTX	CTX + AgNPs	CZ	CZ + AgNPs
A. baumannii	6	12 ± 0.8	6	11 ± 0.6	6	11 ± 0.8
K. pneumonia	6	11 ± 0.4	6	11 ± 0.4	6	10 ± 0.6
P. aeruginosa	6	10 ± 0.7	6	10 ± 0.9	6	10 ± 0.4

CIP, ciprofloxacin; CTX, cefotaxime; CZ, cefazolin

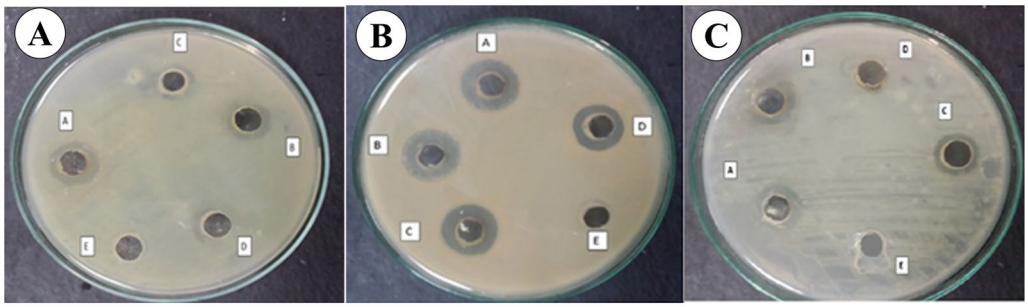

Fig. 9 Effect of AgNPs on pathogenic bacteria *A. baumannii* (**A**), *P. aeruginosa* (**B**), *K. pneumoniae* (**C**), well A: AgNPs 1 mM $AgNO_3$ and pH 7, well B: AgNPs 2 mM $AgNO_3$ and pH 7, Well C: AgNPs 4 Mm $AgNO_3$ and pH 7, Well D: AgNPs 1 Mm $AgNO_3$ and pH 8, Well E: silver nitrate solution as control

Table 7 MIC and MBC of *P. aeruginosa* AgNPs concentration (mg/ml) on *A. baumannii, K. pneumoniae* and *P. aeruginosa*

Bacterial strains	*A. baumannii*		*K. pneumonia*		*P. aeruginosa*	
	MIC	MBC	MIC	MBC	MIC	MBC
P. aeruginosa AgNPs concentration (mg /l)	100	150	100	150	100	150

Table 8 Cell viability percent of hepatocellular carcinoma cell line treated with silver nanoparticles

	Nanoparticles ug/ml	Cell viability %
Concentration	10	94.9675 ± 0.81215
	100	19.7522 ± 2.307
LC 50%	60.584	50

The minimum inhibitory concentration (MIC) and minimum bacterial concentration (MBC)

The biosynthesized AgNPs from the bacterial metabolites of *P. aeruginosa* recoded 1 mg/ml for the MIC and 1.5 mg/ml for MBC with *K. pneumoniae, P. aeruginosa,* and *A. baumannii* (Table 7). This result agreed with the MICs of AgNPs were recoded to be 3.125 mg/ml against *K. pneumoniae* and 1.56 mg/ml against *P. aeruginosa*. Additionally, they mentioned that the GNB recorded the MIC up to 150–600 mg/L by using AgNPs.

Cytotoxicity assay of silver nanoparticles in vitro

Cancer treatment by nanomedicine is promising, hepatocellular carcinoma (HCC) Incidence is increasing worldwide, and it is considered cancer the main cause of death. This experiment evaluates the cytotoxic effect of AgNPs synthesized from the metabolites of *P. aeruginosa* in HepG2 cells. The cytotoxic effect at a concentration 10 µg/ml was 94.9675, and the concentration of 100 µg/ml has a higher cytotoxic effect for cell viability 19.7522 by calculation LC 50% will be 62.307 µg/ml (Table 8).

Discussion

Antibiotic resistance is one global crisis annually, especially after increasing the types of resistant microorganisms and antibiotic types that are resisted by microbes, particularly inside the ICU due to the weak immune system of patients in these units. According to the Extended Prevalence of Infection in Intensive Care (EPIC) II study, 51% of patients were infected in the ICU and the major

cases up to 64% were infected through the respiratory origin, and most of the infected bacteria were GNB (62.2%) [1]. The MDR bacteria were recently classified to GPB and GPB. The current results in Table 1 confirmed that the high percentage of pathogenic bacteria in ICU patient's cultures were GNP. These results matched the previous result that recorded more than 80% of the pathogens in the ICU were classified as *Enterococcus faecium, Enterobacter* spp., *A. baumannii, K. pneumoniae, P. aeruginosa, and Staph. aureus* [2]. The coloration of the mixture was the primary indicator to confirm the biosynthesis of AgNPs from the mixture of $AgNO_3$. Color transition of the bacterial supernatants from yellow to brown gives an indication of the biosynthesis process by biotransformation of Ag^+ ion to Ag^0. The reduction of Ag^+ ions could be carried out by the metabolic products of the bacterial cell, such as proteins, amino acids, and / or extracellular enzymes. Contrary, the color of the control experiments did not change, confirming that the metabolites byproducts of *P. aeruginosa* are responsible for the reduction of Ag^+ in the biosynthesis process and not the media components. The second confirmation test was the spectroscopy measurement of the UV–vis absorption intensity to confirm the mutual vibrations of the surface plasmon resonance (SPR) in the nanometals as in Fig. 3. The confirmed peak of SPR was reported at the absorption between 400 and 450 nm. The current findings matched with the UV–vis spectra of biosynthesized spherical AgNPs, which reported a single, strong, and broad peak at 400 nm [7, 30]. Furthermore, the same absorption peak was recorded at 390 nm from *A. baumannii* [31], broad peak at 405–407 nm with supernatant of *K. pneumoniae* [32], a broad absorption peak was determined at 420 nm by supernatant of *P. aeruginosa* [33], and a single peak was observed at 440 nm with *A. calcoaceticus* LRVP54 [24]. The biosynthesis of AgNPs was reported using fungus species such as *Fusarium oxysporum* and discovered the reduction agents of Ag^+ ion were the proteins, mainly NADH-dependent reductase [34]. This was also confirmed by Monowar et al., who studied the effect of secondary metabolites of endophytic *A. baumannii* and *P. aeruginosa,* especially the phenolic compounds as antioxidant agents, on the formation of AgNPs from silver nitrate solution [35].

To reach the optimum conditions for AgNPs biosynthesis, the bacterial supernatant was used at different volumes, representing the master key to controlling the size and shape of AgNPs. It has effects on the reaction time and color of the reaction mixture. Figures 4 and 5 show that the reaction mixture containing 50% supernatant had the higher absorbance intensity than 25% and 10% of supernatant volume. The absorbance intensity was increased by increasing the volume of bacterial supernatant as an indicator to increase the biosynthesis of AgNPs, as seen in Fig. 5. The high production rate of AgNPs at 50% could be related to the high concentration of the secondary metabolites and enzymes in cell-free supernatant of *P. aeruginosa*.

The second key in the biosynthesis process was the concentration of $AgNO_3$, and the maximum intensity was recorded at 4 mM concentration of $AgNO_3$ in the three-mixture volume of the supernatant as in Fig. 6, which indicates that $AgNO_3$ concentration has directly proportional to nanoparticles formation from the biosynthesis process-based *P. aeruginosa.* This finding confirms the effect of the bacterial supernatant, as increasing the concentration of silver ions requires an increase in reducing agents such as enzymes to reach the maximum reduction degree of silver ions.

These results confirm the results obtained from increasing the volume of the mixture, as increasing the concentration of Ag^+ ion requires a high concentration of the reducing agents such as secondary metabolites. Also, enzymes saturate the Ag^+ ion and reach the maximum reduction degree of silver ions, based on the enzyme–substrate kinetics of the active biomolecule site. The same strain of *P. aeruginosa* for the biosynthesis of AgNPs was reported with the same finding; the AgNPs production was increased with increasing $AgNO_3$ concentrations, till 3.0 mM $AgNO_3$ (0.389). After that, the production of AgNPs started to decrease gradually by increasing the concentrations of $AgNO_3$ [36]. In contrast, Wadhwani et al. found the maximum reduction of silver ions in the biosynthesis process of AgNPs was at the lowest concentration of $AgNO_3$ (0.5 and 0.7 mM), and the lost reduction of Ag^+ ion was obtained at a high concentration of $AgNO_3$ (5 mM) [24].

The third factor was the pH of the biosynthesis reaction, which directly affects biosynthesis of AgNPs as each enzyme has a particular pH range and any change in the pH will affect the activity of bacterial enzymes as in Fig. 7. Extreme pH values can cause denaturation of enzymes and reduce the binding parts of the biomolecules due to the changing of the electrical charges of silver metals, as in Fig. 7. A general trend is to get the SPR and the shifting of peak toward the short wavelength region become narrower by increasing the pH value. Alqadi et al. found an inverse correlation between the pH and the size of the synthesized particles, increasing the pH of the small size of the AgNPs [37]. Furthermore, the reduction in AgNPs size was identified by shifting the peak and the shorter wavelength. Abo-State and Partila reported that the most efficient pH in nanoparticle biosynthesis from *P. aeruginosa* was pH 7 [36]. This result is matching with current results at pH 8. The UV–vis absorbance was less than pH

7 and smaller particle size, while pH 4 is unsuitable for enzyme interaction [37].

The morphological characteristics of the biosynthesized AgNPs were identified using TEM analysis. The AgNPs particles were characterized by their homogeneity in size (11–29 nm) and spherical shape. In the same context, these results are consistent with the reported data by Wadhuani et al., who found the TEM analyses of polydisperse AgNPs from 1 mM $AgNO_3$ of 10–60 nm in size after 168 h [24]. Also, Wan et al., synthesized the AgNPs in size of 5–12 nm, in addition to its stability for more than 6 month at 37 °C [30]. While Shaker and Shaaban reported that the biosynthesized AgNPs have hetero shapes (spherical and square) ranging between 37 and 168 nm in diameter [31]. Likewise, Singh et al. synthesized irregular shapes of the AgNPs from *P. aeruginosa* in size of 10–40 nm [38].

The X-ray diffraction of AgNPs-based *P. aeruginosa* identified the diffraction patterns of metallic silver at 2 θ values of 27.153°, 32.323°, 38.018°, 64.35°, and 43.934° (Fig. 9). This pattern confirmed the metallic structure of AgNPs in face-centered-cubic (FCC). These results were in the same context as the reported database of JCPDS file no 03-092. Furthermore, Singh et al. investigated the XRD pattern of synthesized AgNPs from *P. aeruginosa* at 2θ values (20–82°), which consisted of five peaks at 38.116°, 44.227°, 64.426°, 77.472°, and 81.536°, these peaks corresponding to the 111, 200, 220, 311 and 222 orientations, respectively. The value of 2θ between 20° to 82° confirmed the crystalline structure of the biosynthesized AgNPs according to the standards spectrum (JCPDS file no 04-0783) [38].

The FTIR analysis confirmed the responsibility of the amino acids and proteins in the metabolites of *P. aeruginosa* to stabilize the AgNPs via the carboxylate ion (COO^-) [39]. In this regard, it can be stated that the FTIR spectrum can establish the presence of capping amino acids and protein around the AgNPs synthesized from the bacterial supernatant of *P. aeruginosa*.

The activity of biosynthesized AgNPs as antimicrobial agents to inhibit the growth of MDR bacteria *A. baumannii, K. pneumonia,* and *P. aeruginosa* using well diffusion assay. AgNPs have higher antibiotic efficacy when combined with antibiotic disc due to its destruction of cell walls and facilitating antibiotics entrance inside bacterial cells. The antibacterial activity of AgNPs against pathogenic organisms has extensively studied and reported [7, 38, 40], they reported the mode of action of antibacterial effects due to the small size with the large surface area of AgNPs can be attached to the cell membrane or break through it, and the toxicity of AgNPs was increased with decreasing the particle size. The alternative mechanism refers to the formation of free radicals which can break the membrane lipids, peptidoglycan, DNA, and protein, which can cause damage, dissociation and inhibit the growth of the bacterial cell [12]. Quinteros et al. report that the AgNPs generated or in *P. aeruginosa, E. coli,* and *Staph. aureus* mediated, and that was correlated with inhibition of the microbial growth [41]. Moreover, the antimicrobial activity of biosynthesized AgNPs from *P. aeruginosa* [41] and *E. coli* [42] were also studied against opportunistic microorganisms and human pathogens and they found the better effect of AgNPs recorded in combined with antibiotics against microbes [43]. The synergistic antibacterial effects of AgNPs with commercial antibiotics were extensively studied against different pathogenic bacteria such as *Staph. aureus* by using neomycin and gentamicin with AgNPs [44]. Similarly, Qaralleh group's and Nikparast and Saliani reported the maximum synergistic effect against *Staph. epidermidis*, *Staph. aureus*, *P. aeruginosa* and *E. coli* was recorded by the combination of the antibiotics such as ciprofloxacin, trimethoprim, cefotaxime, ampicillin, tetracycline, and gentamicin with AgNPs and/or essential oils [40, 45]. Finally, the anticancer and cytotoxicity efficacy of AgNPs was evaluated by (SRB assay) on Hep G2 Hepatocellular carcinoma cell line, and LC 50% is 60.584 µg/ml. This result agreed with Vijayakumar et al., who used chitin extracted from shrimp shells as a reducing agent to synthesize AgNPs. Also, the anticancer and cytotoxicity activity of biosynthesized AgNPs were examined on human hepatocellular carcinoma (HepG2), and the value of IC50 was 57 ± 1.5 µg/ml [20]. Wan et al. investigated the effect of $AgNO_3$ at the different concentrations on the AgNPs and their cytotoxic effects on cell growth. They found that the high concentration of AgNPs has insignificant cytotoxicity in A549 and HL-7702 cells, especially at higher concentrations than 10 µg/mL. These results approved current results and confirmed that the cytotoxicity effect of $AgNO_3$ is higher than AgNPs [30]. Alongside, Raj et al. investigated the cytotoxicity of β-sitosterol-assisted AgNPs (BSS-SNPs) in HepG2 cells, the AgNPs have high cytotoxic activity, and the IC50 was 7 ng/mL of BSS-SNPs in HepG2 cells [46].

Conclusions

Nanotechnology is the most promising solution to combat presence of multi-drug resistance, especially in the ICU. Cell-free filtrate of *P. aeruginosa* containing reducing agent can reduce and capping $AgNO_3$ to AgNPs with significant antibacterial activity alone and/or has a potential synergistic action with other antibiotics. Also, the AgNPs has considered as promising therapeutic option as anticancer against the hepatocellular carcinoma. It is worth noting that the productivity of nano-silver needs

more future studies to find the optimal conditions to obtain the highest productivity and the best specifications with a better effect against pathogenic MDR and various cancer cell lines.

Acknowledgements
The authors would like to acknowledge University of Sadat City-Egypt, National Liver Institute, Menoufia University-Egypt, and Cairo University-Egypt.

Author contributions
Conceptualization, ABAM, MMA, MKMK, ASA and RNA; methodology, ABAM, MMA, MKMK, ASA and RNA; software, MMA and MKMK; validation, ABAM, MMA, MKMK, ASA and RNA; formal analysis, ABAM, MMA, MKMK, ASA and RNA; investigation, ABAM, MMA, MKMK, ASA and RNA; resources, ABAM and MMA; data curation, ABAM, MMA, MKMK, ASA and RNA; writing—original draft preparation, ABAM, MMA and RHA; writing—review and editing, ABAM and ASA; visualization, ABAM, RNA and ASA; supervision, ABAM, MKMK, ASA and RNA. All authors read and approved the final manuscript.

Funding
This research received no external funding. Open access funding provided by The Science, Technology & Innovation Funding Authority (STDF) in cooperation with The Egyptian Knowledge Bank (EKB).

Availability of data and materials
The data are ready when requested.

Declarations

Ethics approval and consent to participate
Not applicable.

Consent for publication
Not applicable.

Competing interests
The authors have not declared any conflict of interests.

Author details
[1]Department of Microbial Biotechnology, Genetic Engineering and Biotechnology Research Institute, University of Sadat City, Sadat, Egypt. [2]National Liver Institute, Menoufia University, Shebin El-Kom 32511, Egypt. [3]Anesthesia and Intensive Care Department, National Liver Institute, Menoufia University, Shebin El-Kom 32511, Egypt. [4]Department of Microbiology, Faculty of Agriculture, Cairo University, Giza 12613, Egypt.

Received: 25 May 2022 Accepted: 2 October 2022
Published: 4 November 2022

References

1. Vincent J-L, Rello J, Marshall J et al (2009) International study of the prevalence and outcomes of infection in intensive care units. JAMA 302:2323. https://doi.org/10.1001/jama.2009.1754
2. Peterson LR (2009) Bad bugs, no drugs: no ESCAPE revisited. Clin Infect Dis 49:992–993. https://doi.org/10.1086/605539
3. Gurunathan S, Park JH, Han JW, Kim JH (2015) Comparative assessment of the apoptotic potential of silver nanoparticles synthesized by Bacillus tequilensis and Calocybe indica in MDA-MB-231 human breast cancer cells: Targeting p53 for anticancer therapy. Int J Nanomed 10:4203–4223. https://doi.org/10.2147/IJN.S83953
4. Mendrek B, Chojniak J, Libera M et al (2017) Silver nanoparticles formed in bio- and chemical syntheses with biosurfactant as the stabilizing agent. J Dispers Sci Technol 38:1647–1655. https://doi.org/10.1080/01932691.2016.1272056
5. Bansal M, Bansal A, Sharma M, Kanwar P (2015) Green Synthesis of Gold and Silver Nanoparticles. Res J Pharm Biol Chem Sci 6(3):1710–1716
6. Wu W, Jin Y, Bai F, Jin S (2015) Pseudomonas aeruginosa. Mol Med Microbiol Second Ed 2–3:753–767. https://doi.org/10.1016/B978-0-12-397169-2.00041-X
7. Mohammed ABA, Mohamed A, El-Naggar NE-A et al (2022) Antioxidant and antibacterial activities of silver nanoparticles biosynthesized by *Moringa oleifera* through response surface methodology. J Nanomater 2022:9984308. https://doi.org/10.1155/2022/9984308
8. Bindhu MR, Umadevi M, Esmail GA et al (2020) Green synthesis and characterization of silver nanoparticles from Moringa oleifera flower and assessment of antimicrobial and sensing properties. J Photochem Photobiol B Biol. https://doi.org/10.1016/j.jphotobiol.2020.111836
9. Prasad TNVKV, Elumalai EK (2011) Biofabrication of Ag nanoparticles using Moringa oleifera leaf extract and their antimicrobial activity. Asian Pac J Trop Biomed 1:439–442. https://doi.org/10.1016/S2221-1691(11)60096-8
10. Chen Y, Duan X, Zhou X et al (2021) Advanced oxidation processes for water disinfection Features, mechanisms and prospects. Chem Eng J. https://doi.org/10.1016/j.cej.2020.128207
11. Reidy B, Haase A, Luch A et al (2013) Mechanisms of silver nanoparticle release, transformation and toxicity: a critical review of current knowledge and recommendations for future studies and applications. Materials 6(6):2295–2350. https://doi.org/10.3390/ma6062295
12. Morones JR, Elechiguerra JL, Camacho A et al (2005) The bactericidal effect of silver nanoparticles. Nanotechnology 16:2346. https://doi.org/10.1088/0957-4484/16/10/059
13. AshaRani PV, Mun GLK, Hande MP, Valiyaveettil S (2009) Cytotoxicity and genotoxicity of silver nanoparticles in human cells. ACS Nano 3:279–290. https://doi.org/10.1021/nn800596w
14. Xue Y, Zhang T, Zhang B et al (2016) Cytotoxicity and apoptosis induced by silver nanoparticles in human liver HepG2 cells in different dispersion media. J Appl Toxicol 36:352–360. https://doi.org/10.1002/jat.3199
15. Baron EJ (2015) Specimen collection, transport, and processing: bacteriology. In: Jorgensen JH, Carroll KC, Funke G, Pfaller MA, Landry ML, Richter SS, Warnock DW (eds) Manual of Clinical Microbiology. DC, USA, Washington
16. Funke G, Funke-Kissling P (2004) Evaluation of the new VITEK 2 card for identification of clinically relevant gram-negative rods. J Clin Microbiol 42:4067–4071. https://doi.org/10.1128/JCM.42.9.4067-4071.2004
17. Bush K, Jacoby GA, Medeiros AA (1995) A functional classification scheme for beta-lactamases and its correlation with molecular structure. Antimicrob Agents Chemother 39:1211–1233
18. Bradford PA (2001) Extended-spectrum β-lactamases in the 21st century: characterization, epidemiology, and detection of this important resistance threat. Clin Microbiol Rev 14:933–951
19. Lee JH, Bae IK, Hee LS (2012) New definitions of extended-spectrum β-lactamase conferring worldwide emerging antibiotic resistance. Med Res Rev. https://doi.org/10.1002/med.20210
20. Vijayakumar M, Priya K, Ilavenil S et al (2020) Shrimp shells extracted chitin in silver nanoparticle synthesis: expanding its prophecy towards anticancer activity in human hepatocellular carcinoma HepG2 cells. Int J Biol Macromol. https://doi.org/10.1016/j.ijbiomac.2020.10.032
21. Kim M, Morrison M, Yu Z (2011) Evaluation of different partial 16S rRNA gene sequence regions for phylogenetic analysis of microbiomes. J Microbiol Methods. https://doi.org/10.1016/j.mimet.2010.10.020
22. Katva S, Das S, Moti HS et al (2018) Antibacterial synergy of silver nanoparticles with gentamicin and chloramphenicol against *Enterococcus Faecalis*. Pharmacogn Mag 13:S828–S833. https://doi.org/10.4103/pm.pm_120_17
23. Klaus T, Joerger R, Olsson E, Granqvist CG (1999) Silver-based crystalline nanoparticles, microbially fabricated. Proc Natl Acad Sci U S A 96:13611–13614. https://doi.org/10.1073/pnas.96.24.13611
24. Wadhwani S, Singh R, Kumbhar A et al (2013) Synthesis, optimization, and characterization of silver nanoparticles from *Acinetobacter calcoaceticus* and their enhanced antibacterial activity when combined with antibiotics. Int J Nanomedicine. https://doi.org/10.2147/ijn.s48913
25. Vijayalakshmi R, Rajendran V (2012) Synthesis and characterization of nano-TiO2 via different methods. Arch Appl Sci Res 4:1183–1190
26. Balouiri M, Sadiki M, Ibnsouda SK (2016) Methods for in vitro evaluating antimicrobial activity: a review. J Pharm Anal 6:71–79. https://doi.org/10.1016/J.JPHA.2015.11.005

27. EUCAST E (2003) Determination of minimum inhibitory concentrations (MICs) of antibacterial agents by broth dilution. Clin Microbiol Infect 9:ix–xv. https://doi.org/10.1046/j.1469-0691.2003.00790.X
28. Skehan P, Storeng R, Scudiero D et al (1990) New colorimetric cytotoxicity assay for anticancer-drug screening. J Natl Cancer Inst 82:1107–1112. https://doi.org/10.1093/jnci/82.13.1107
29. Chirgadze YN, Fedorov OV, Trushina NP (1975) Estimation of amino acid residue side-chain absorption in the infrared spectra of protein solutions in heavy water. Biopolymers 14:679–694. https://doi.org/10.1002/bip.1975.360140402
30. Wan G, Ruan L, Yin Y et al (2016) Effects of silver nanoparticles in combination with antibiotics on the resistant bacteria *Acinetobacter baumannii*. Int J Nanomedicine 11:3789–3800. https://doi.org/10.2147/IJN.S104166
31. Shaker MA, Shaaban MI (2017) Synthesis of silver nanoparticles with antimicrobial and anti-adherence activities against multidrug-resistant isolates from *Acinetobacter baumannii*. J Taibah Univ Med Sci 12:291–297. https://doi.org/10.1016/j.jtumed.2017.02.008
32. Kalpana D, Lee YS (2013) Synthesis and characterization of bactericidal silver nanoparticles using cultural filtrate of simulated microgravity grown *Klebsiella pneumoniae*. Enzyme Microb Technol 52:151–156. https://doi.org/10.1016/j.enzmictec.2012.12.006
33. Quinteros MA, Cano Aristizábal V, Dalmasso PR et al (2016) Oxidative stress generation of silver nanoparticles in three bacterial genera and its relationship with the antimicrobial activity. Toxicol Vitr 36:216–223. https://doi.org/10.1016/j.tiv.2016.08.007
34. Ahmad A, Mukherjee P, Senapati S et al (2003) Extracellular biosynthesis of silver nanoparticles using the fungus *Fusarium oxysporum*. Colloids Surfaces B Biointerfaces 28:313–318. https://doi.org/10.1016/S0927-7765(02)00174-1
35. Monowar T, Rahman MS, Bhore SJ et al (2019) Secondary metabolites profiling of acinetobacter baumannii associated with chili (*Capsicum annuum L.*) leaves and concentration dependent antioxidant and prooxidant properties. Biomed Res Int. https://doi.org/10.1155/2019/6951927
36. AboState MA, Partila AM (2015) Microbial production of silver nanoparticles by *Pseudomonas Aeruginosa* cell free extract. J Ecol Heal Environ. https://doi.org/10.12785/jehe/030306
37. Alqadi MK, Abo Noqtah OA, Alzoubi FY et al (2014) PH effect on the aggregation of silver nanoparticles synthesized by chemical reduction. Mater Sci Pol 32:107–111. https://doi.org/10.2478/s13536-013-0166-9
38. Singh H, Du J, Singh P, Yi TH (2018) Extracellular synthesis of silver nanoparticles by *Pseudomonas* sp. THG-LS1.4 and their antimicrobial application. J Pharm Anal 8:258–264. https://doi.org/10.1016/J.JPHA.2018.04.004
39. Coates J (2006) Interpretation of Infrared Spectra A Practical Approach. In: Meyers RA (ed) Encyclopedia of Analytical Chemistry: Applications, Theory and Instrumentation. Chichester, UK, John Wiley & Sons Ltd
40. Nikparast Y, Saliani M (2018) Synergistic effect between phyto-synthesized silver nanoparticles and ciprofloxacin antibiotic on some pathogenic bacterial strains. J Med Bacteriol 7(2):36–43
41. Quinteros MA, Aiassa Martínez IM, Dalmasso PR, Páez PL (2016) Silver nanoparticles: biosynthesis using an ATCC reference strain of *Pseudomonas aeruginosa* and activity as broad spectrum clinical antibacterial agents. Int J Biomater 2016:1–7. https://doi.org/10.1155/2016/5971047
42. Koilparambil D, Kurian LC, Vijayan S, Manakulam Shaikmoideen J (2016) Green synthesis of silver nanoparticles by *Escherichia* coli: analysis of antibacterial activity. J Water Environ Nanotechnol 1:63–74. https://doi.org/10.7508/jwent.2016.01.008
43. Gandhi H, Khan S (2016) Biological synthesis of silver nanoparticles and its antibacterial activity. J Nanomed Nanotechnol 07:2–4. https://doi.org/10.4172/2157-7439.1000366
44. Jamaran S, Zarif BR (2016) Synergistic effect of silver nanoparticles with neomycin or gentamicin antibiotics on mastitis-causing *Staphylococcus aureus*. Open J Ecol 6:452–459
45. Qaralleh H, Khleifat KM, Al-Limoun MO et al (2019) Antibacterial and synergistic effect of biosynthesized silver nanoparticles using the fungi *Tritirachium oryzae* W5H with essential oil of Centaurea damascena to enhance conventional antibiotics activity. Adv Nat Sci Nanosci Nanotechnol 10:25016
46. Raj RK, Ezhilarasan D, Rajeshkumar S (2020) β-Sitosterol-assisted silver nanoparticles activates Nrf2 and triggers mitochondrial apoptosis via oxidative stress in human hepatocellular cancer cell line. J Biomed Mater Res—Part A 108:1899–1908. https://doi.org/10.1002/jbm.a.36953

Publisher's Note

Springer Nature remains neutral with regard to jurisdictional claims in published maps and institutional affiliations.

Submit your manuscript to a SpringerOpen journal and benefit from:

- ► Convenient online submission
- ► Rigorous peer review
- ► Open access: articles freely available online
- ► High visibility within the field
- ► Retaining the copyright to your article

Submit your next manuscript at ► springeropen.com